Contents

Laser-Assisted Magnetic Resonance: Principles and Applications

Dieter Suter and Jörg Gutschank

Universität Dortmund, Fachbereich Physik, 44221 Dortmund, Germany,
dieter.suter@physik.uni-dortmund.de

Summary. Laser radiation can be used in various magnetic resonance experiments. This chapter discusses a number of cases, where laser light either improves the information content of conventional experiments or makes new types of experiments possible, which could not be performed with conventional means. Sensitivity is often the main reason for using light, but it also allows one to become more selective, e.g. by selecting signals only from small parts of the sample. Examples are given for NMR, NQR, and EPR spectra that use were taken with the help of coherent optical radiation.

1 Introduction

The interest in the field of magnetic resonance spectroscopy is based largely on the huge potential for applications: spins can serve as probes for their environment because they are weakly coupled to other degrees of freedom. In most magnetic resonance experiments, these couplings are used to monitor the environment of the nuclei, like spatial structures or molecular dynamics.

While the direct excitation of spin transitions requires radio frequency or microwave irradiation, it is often possible to use light for polarizing the spin system or for observing its dynamics. This possibility arises from the coupling of spins with the electronic degrees of freedom: optical photons excite transitions between states that differ both in electronic excitation energy as well as in their angular momentum states.

1.1 Motivation

Some motivations for using light in magnetic resonance experiments include

- Sensitivity: In many cases, the possible sensitivity gains are the primary reason for using optical methods. Compared to conventional NMR, sensitivity gains of more than 10 orders of magnitude are possible. The ultimate

limit in terms of sensitivity was reached in 1993, when two groups showed that it is possible to observe EPR transitions in single molecules [1, 2]. The same technique was later used to observe also NMR transitions in a single molecule [3].

- Selectivity: Lasers can be used to selectively observe signals from specific parts of the sample, like surfaces, at certain times which may be defined by laser pulses with a resolution of 10^{-14} s, or from a particular chemical environment defined, e.g. by the chromophore of a molecule or the quantum confined electrons in a semiconductor.
- Speed: Magnetic resonance requires the presence of a population difference between spin states to excite transitions between them. In conventional magnetic resonance, this population difference is established by thermal relaxation through coupling with the lattice, i.e. the spatial degrees of freedom of the system. At low temperatures, this coupling process may be too slow for magnetic resonance experiments. In the case of optical excitation, the population differences are established by the polarizing laser light. Depending on the coupling mechanism, this polarization process can be orders of magnitude faster than the thermal polarization process, independent of temperature.
- Electronically excited states: If information about an electronically excited state is desired that is not populated in thermal equilibrium, it may be necessary to use light to populate this state. It is then advantageous to populate the different spin states unequally to obtain at the same time the polarization differences that are needed to excite and observe spin transitions.

1.2 What Can Lasers Do?

Light can support magnetic resonance experiments in different ways. They can, e.g., initiate a chemical reaction that one wishes to observe, like in photosynthetic processes. These light-induced modifications of the sample will not be considered here; instead we concentrate on the use of light for the magnetic resonance experiment, where light affects directly the spin degrees of freedom, rather than spatial coordinates. Typically, the laser is then used either to increase or to detect the spin polarization of nuclear or electronic spins.

These two approaches are largely independent of each other: It is, e.g., possible to use optical pumping to enhance the spin polarization and observe the transitions with a conventional NMR coil; conversely, optical detection can be used with or without increasing the population difference with laser light. In many cases, however, it is advantageous to combine both approaches. In some cases, a single laser beam may provide an increase of the spin polarization and an optical signal that can be related to a component of the magnetization. In others, a pump-probe setup separates the excitation and detection paths.

In addition to these applications of lasers, light can also be used to drive the dynamics of spin systems, e.g. through Raman transitions [4]. For this review, however, we will concentrate on the issues of increasing the spin polarization and on optical detection.

2 Optical Polarization of Spin Systems

Magnetic resonance spectroscopy requires a spin polarization inside the medium. In conventional magnetic resonance experiments, this polarization is established by thermal contact of the spins with the lattice. This process is relatively slow, especially at low temperatures, where relaxation times can be many hours, and it leads to polarizations that are limited by the Boltzmann factor. Photon angular momentum, in contrast, can be created in arbitrary quantities with a polarization that can be arbitrarily close to unity. If it is possible to transfer this polarization to nuclear or electronic spins, their polarization can increase by many orders of magnitude.

A number of different approaches have been used to achieve this goal. The oldest and best known approach is known as optical pumping [5]; it was originally demonstrated on atomic vapors [6] and later applied to condensed matter. While optical pumping allows one to create very high spin polarization in atomic vapors, it is less suitable for applications to anisotropic systems such as low symmetry solids. Other techniques were therefore developed, which can still be used in such an environment. While optical pumping was originally implemented with conventional light sources, most of the other approaches require the use of coherent optical radiation, i.e. laser light.

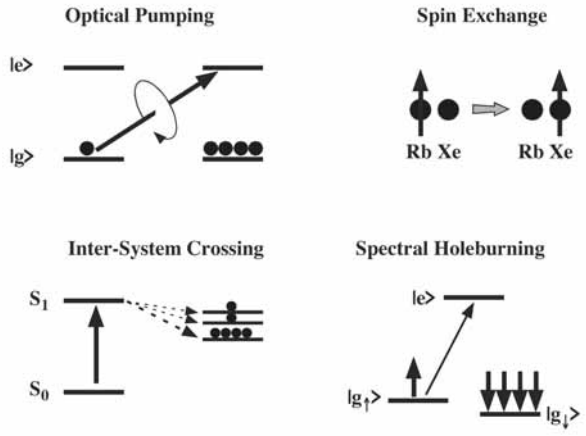

Fig. 1. Four ways for optically increasing the spin polarization.

2.1 Optical Pumping

The possibility to use optical radiation for exciting and detecting spin polarization can be traced back to the angular momentum of the photon. Photons as the carriers of the electromagnetic interaction carry one unit ($\hbar$) of angular momentum, which is oriented either parallel or antiparallel to the direction of propagation of the light. In an isotropic environment, angular momentum is a conserved quantity. When a photon is absorbed by an atom or molecule, its angular momentum must therefore be transferred to the atom. The resulting angular momentum of the atom is equal to the vector sum of its initial angular momentum plus the angular momentum of the absorbed photon.

The use of angular momentum conservation for increasing the population difference between spin states was first suggested by Alfred Kastler [7, 8, 5]. If an atom is irradiated by circularly polarized light, the photons have a spin quantum number $m_s = +1$. Since the absorption of a photon is possible only if both, the energy and the angular momentum of the system are conserved, the atoms can only absorb light by simultaneously changing their angular momentum state by one unit.

After the atom has absorbed a photon it will reemit one, decaying back into the ground state. Spontaneous emission can occur in an arbitrary direction in space and is therefore not limited by the same selection rules as the excitation process with a laser beam of definite direction of propagation. The spontaneously emitted photons carry away angular momentum with different orientations and the atom can therefore return to a ground state whose angular momentum state differs by $\Delta m = 0, \pm 1$. The net effect of the absorption and emission processes is therefore a transfer of population from one spin state to the other and thereby a polarization of the atomic system.

2.2 Spin Exchange

Spin polarization can be transferred between different reservoirs not only within one atomic species, but also between different particles. This was first demonstrated by Dehmelt who used transfer to free electrons to polarize them [9]. Another frequently used transfer process uses optical pumping of alkali atoms, in particular Rb and Cs and transfer of their spin polarization to noble gas atoms like Xe. These atoms cannot be optically pumped from their electronic ground state (although He can be pumped in the metastable state [10, 11]); spin exchange allows one to optically pump an alkali gas (typically rubidium) and transfer the spin polarization from there to the Xe nuclear spin. This method was pioneered by Happer [12], applied to the study of surfaces [13, 14], and used in a number of medical applications [15, 16, 11].

The transfer from alkali to noble gas atoms is relatively efficient when the two species form van der Waals complexes. During the lifetime of this quasi-molecule, the two spins couple, mainly by dipole-dipole interaction. This

coupling allows simultaneous spin flips of the two species which transfer polarization from the Rb atoms to the Xe nuclear spin. Typical cross-polarization times are on the order of minutes, but the long lifetime of the Xe polarization permits to reach polarizations close to unity. The spin polarization survives freezing [17] and can be transferred to other spins by thermal mixing [18].

2.3 Excited Triplet States

In many classical optically detected magnetic resonance experiments, absorption of light excites the system into a singlet state that can, through nonradiative processes, decay into a triplet state, whose energy is below the excited singlet state. This intersystem conversion process as well as the decay of the triplet state can be spin-dependent, therefore creating a significant spin polarization of the triplet state. In many systems, these processes are quite efficient, even for unpolarized light, generating a high degree of spin polarization in the triplet state. Under certain conditions, this polarization of the electron spin can also lead to a polarization of the nuclear spin, which survives when the molecule returns to its ground state.

2.4 Spectral Holeburning

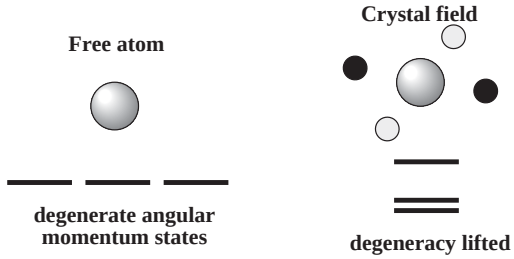

Fig. 2. Quenching of angular momentum by interaction with the crystal field.

When the spin is located in a host material with low symmetry, the electronic angular momentum is quenched. Figure 2 shows the situation schematically: While angular momentum states with total angular momentum J are $2J + 1$ fold degenerate in free space, the Coulomb interaction of the atom or ion with neighboring charges (electrons and nuclei) lifts this degeneracy. The resulting states are usually no longer angular momentum eigenstates. While this argument applies directly only to orbital angular momentum, the spin-orbit interaction often is strong enough to also quench the electron spin.

If the angular momentum is quenched, optical pumping with circularly polarized light becomes inefficient for excitation of spin polarization. In these

systems, other approaches may increase spin polarization. One possibility exists when the different spin states can be distinguished in frequency space, i.e. when the energy difference between them is larger than the homogeneous width of a suitable optical transition. The situation is shown schematically in the lower right of figure 1: The laser only excites those ground state atoms whose spin is in the $\uparrow$ state. Since the excited state can decay to both ground states, the population accumulates in the $|g_\downarrow\rangle$ state. This allows one to use a laser to selectively depopulate one of the spin states, while increasing the population of the other states.

Since the inhomogeneous width of the optical transitions is usually large compared to the energy of magnetic resonance transitions, it is rarely possible to address only a single spin state. The laser frequency selects then a subset of all the spins, for which the resonance condition is fulfilled; only for those systems, the spin polarization will be increased. This situation is known as spectral holeburning, since the depopulation of specific spin states reduces the absorption of light at the frequency of the pump laser beam. Additional details are discussed in the context of optical detection.

3 Optical Detection

Any magnetic resonance experiment includes a scheme for detection of time-dependent components of the spin polarization, usually as a macroscopic magnetization. In NMR, the precessing transverse magnetization changes the magnetic flux through the radio frequency (rf) coil. According to Faraday's law, the time derivative of the flux induces a voltage over the coil, which is detected as the free induction decay (in pulsed experiments) or as a change in the impedance of the coil (in continuous wave experiments).

The optical detection schemes that we discuss here can sometimes replace this inductive detection. They can be used together with optical polarization or they can be combined with conventional excitation schemes.

In suitable systems, optical detection provides a number of advantages over the conventional method: First, optical radiation introduces an additional resonance condition, which can be used to distinguish different signal components and thereby separate the target signal from backgrounds such as impurities. Second, optical radiation can be detected with single photon sensitivity (in contrast to microwave or radio frequency radiation). This has made detection of single spins possible in suitable systems. A third possible use of the optical radiation is that the laser beam breaks the symmetry of isotropic samples, such as powders or frozen solutions. As we discuss in Section 5.3, this allows one to derive the orientation of tensorial interactions, such as electron g-tensors or optical anisotropy tensors from non-oriented samples.

3.1 Circular Dichroism

An early suggestion that magnetic resonance transitions should be observable in optical experiments is due to Bitter [19]. The physical process used in such experiments may be considered as the complement of optical pumping: the spin angular momentum is transferred to the photons and a polarization selective detection measures the photon angular momentum.

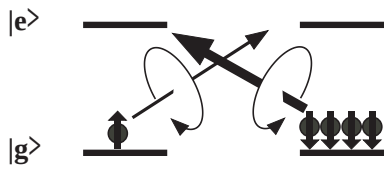

Fig. 3. Optical detection through circular dichroism.

Figure 3 illustrates this for the same model system that we considered for optical pumping. Light with a given circular polarization interacts only with one of the ground state sublevels. Since the absorption of the medium is directly proportional to the number of atoms that interact with the light, a comparison of the absorption of the medium for the two opposite circular polarizations yields directly the population difference between the two spin states. This population difference is directly proportional to the component of the magnetisation parallel to the laser beam.

Early experimental implementations of these techniques were demonstrated in atomic vapors [20, 21, 5], where angular momentum conservation is exact and the principle is directly applicable. Similar considerations hold also for solid materials [22], although, as we discussed above, angular momentum is not always a conserved quantity in such systems. It depends therefore on the symmetry of the material if absorptive detection is possible [23]. Nevertheless, even small optical anisotropies can be measured; changes in these parameters upon saturation of the spins provide a clear signature of magnetic resonance transitions [24].

While most implementations measure the longitudinal spin component by propagating a laser beam parallel to the static magnetic field, it is also possible to observe precessing magnetization with a laser beam perpendicular to the static field [25]. The two approaches provide complementary information [26] and a combination of longitudinal and transverse measurements is therefore often helpful for the interpretation of the spectra.

3.2 Photoluminescence

Photoluminescence is another important tool for measuring spin polarization. Depending on the system, the intensity or the polarization of spontaneously

emitted photons can be a measure of the spin polarization in the ground – or in an electronically excited state. In free atoms, angular momentum conservation imposes correlations between the direction and polarization of the spontaneously emitted photons which depend on the angular momentum state of the excited atom. Photoluminescence has therefore long been used to measure spin polarization in electronically excited states [27, 28].

Spin polarization in the electronic ground state also affects the photoluminescence, since the absorption of polarized light depends on the spin state. If the spin orientation prevents absorption of light, the intensity of the photoluminescence decreases correspondingly. The intensity and polarization of the photoluminescence can therefore serve for detecting ground state spin polarization and, e.g. by saturation with a resonant rf field, for detecting magnetic resonance transitions [29, 30].

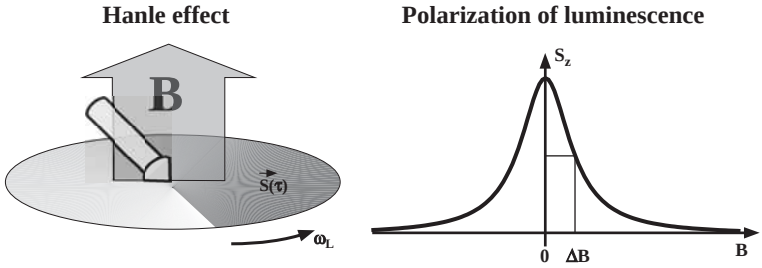

Fig. 4. Hanle effect: A magnetic field perpendicular to a circularly polarized excitation laser forces Larmor precession of the electron spins. The spin polarization of the excited electrons decreases therefore with increasing magnetic field strength.

.

The effect of Larmor precession on the spin polarization of excited states has been observed as early as 1924 by Hanle [31]. He noticed that the polarization of the photoluminescence decreases if a magnetic field is applied perpendicular to the direction of the spin polarization. The observed polarization of the photoluminescence changes with the field B_0 as

$$< S_z >= \frac{\Delta B^2}{\Delta B^2 + B_0^2}, \tag{1}$$

where the width $\Delta B = (\Gamma_r + \Gamma_s)/\gamma$ is determined by the gyromagnetic ratio γ and the relaxation rates Γ_s and Γ_r of the spin and excited state population.

The Hanle effect can also be observed in four-wave mixing experiments [32] in atomic vapors as well as in crystals [33]; in this case, significant polarization of the photoluminescence is only obtained if the crystal has high enough symmetry and mechanical strain is small enough to avoid depolarization. It is particularly suitable for measuring spin polarization in semiconductors with a direct band gap, such as GaAs [34].

3.3 Coherent Raman Scattering

Raman processes are optical scattering processes in which the frequency (and therefore the wavelength) of the scattered light differs from that of the incident light [35]. The energy difference between the incident and the scattered photon is absorbed (or emitted) by excitations of the material in which the scattering occurs. While this excitation of the material is often a vibration, it can also be associated with spin degrees of freedom, in which case the scattering process can be used to detect magnetic resonance transitions.

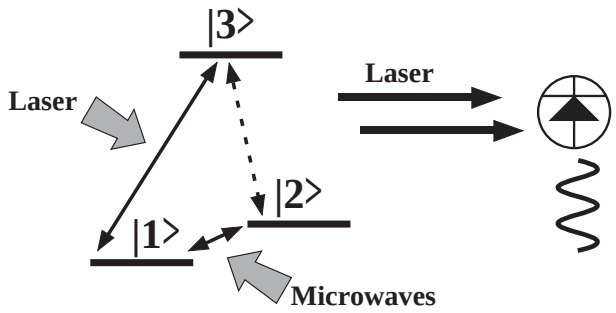

Fig. 5. Coherent Raman scattering from a three-level system. Laser excitation creates a coherence between levels $|1\rangle$ and $|3\rangle$ and microwaves between $|1\rangle$ and $|2\rangle$. The resulting non-linear polarisation in the third transition creates a Raman wave.

Figure 5 shows the relevant process for the simplest possible case: The two states $|1\rangle$ and $|2\rangle$ represent two spin states of the electronic ground state, while $|3\rangle$ is an electronically excited state. If a microwave field (rf in the case of nuclear spin transitions) resonantly excites the transition between states $|1\rangle$ and $|2\rangle$, it creates a coherence between the two spin states. Similarly, the laser excites an optical coherence in the electronic transition $|1\rangle \leftrightarrow |3\rangle$. Since the two transitions share state $|1\rangle$, the two fields create a superposition of all three states, which contains coherences not only in the two transitions that are driven by the external fields, but also in the third transition $|2\rangle \leftrightarrow |3\rangle$. If this transition has a non-vanishing electric dipole moment, this coherence is the source of a secondary optical wave, the Raman field. As the figure shows, the frequency of this wave differs from that of the incident wave by the frequency of the microwave field. It has the same spatial dependence as the incident laser field and therefore propagates in the same direction. If the two optical fields are detected on a usual photodetector (photodiode or photomultiplier), they interfere to create a beat signal at the microwave frequency.

The type of scattering process used for magnetic resonance detection is referred to as "coherent" Raman scattering [36] since the Raman field is phase-coherent with the microwave as well as with the incident laser field. This is an important prerequisite for the detection process: If the laser frequency

drifts, the frequency of the incident field as well as that of the Raman field are shifted by the same amount. As a result, the difference frequency is not affected and the resolution of the measurement is not affected by laser frequency jitter or broad optical resonance lines [37]. Coherent Raman processes provide therefore a combination of high resolution with high sensitivity.

Like in conventional magnetic resonance experiments, the excitation of the magnetic resonance transition indicated in Fig. 5 can be performed either in a continuous (cw) [38] or pulsed [39, 40] mode. Furthermore, the microwave or rf field can be replaced by optical fields, applied to the two electronic transitions, that can excite the spin coherence by another Raman process [41, 42, 43].

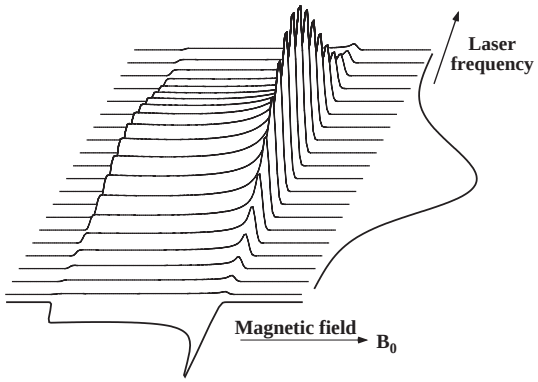

Fig. 6. Two-dimensional optically detected EPR (ODEPR) spectrum as a function of the laser frequency and the magnetic field strength. The result is a complete microwave resonance spectrum for each laser wavelength. The projections on the axes represent the conventional EPR and absorption spectra.

Since the coherence that generates the signal is excited by two resonant fields, it depends on the frequencies of both fields. As shown in Figure 6, the resulting signal is doubly resonant and contains therefore information about the optical as well as the magnetic resonance transition. As with other two-dimensional experiments, it allows one to correlate information from the two frequency dimensions. Examples that demonstrate this feature will be discussed in section 5. While we have discussed the process here as involving magnetic resonance transitions in the ground state, equivalent processes are also possible that relate to spins of electronically excited states.

3.4 Spectral holeburning

In section 2.4, we discussed how narrowband lasers that cause spectral holeburning can increase the polarization of spins, in analogy to optical pumping. In most such experiments, a second laser beam, whose frequency can be swept

around the frequency of the pump beam, is used to monitor the changes in the populations. The resulting spectra are known as holeburning spectra [44].

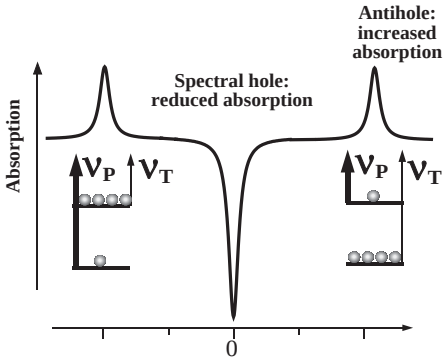

Fig. 7. Schematic representation of a holeburning spectrum. The hole represents reduced absorption, the "antiholes" increased absorption. The separation between hole and antihole is equal to the transition frequency of the two spin states.

As shown in Figure 7, holeburning requires a pump and a probe laser beam. The pump laser modifies the population of those atoms for which the laser frequency matches an electronic transition frequency. When the probe laser hits the same transition, the absorption is reduced in line with the smaller population of the relevant ground state. The population that has been removed from this state is accumulated in the other spin state. When the probe laser frequency is tuned to the transition from this ground state to an electronically excited state, it finds increased absorption, which is referred to as an "antihole". The separation between the hole and antihole matches the energy difference between the two spin states and the hole burning spectrum can therefore measure magnetic resonance transition frequencies [45]. While this discussion has centered on spin transitions between electronic ground states, the procedure also allows one to measure energy differences between spin states of electronically excited states [46].

The optical detection techniques discussed here were chosen to represent the most frequently used approaches. There are several additional techniques which cannot be discussed, which include purely optical techniques like photon echo modulation [47, 48]

4 Applications to NMR and NQR

4.1 Rare earth ions

Ions of rare earth elements have been studied extensively with high resolution optical spectroscopy [49, 50]. The relevant optical transitions are between f electron states and have relatively small homogeneous and inhomogeneous broadening.

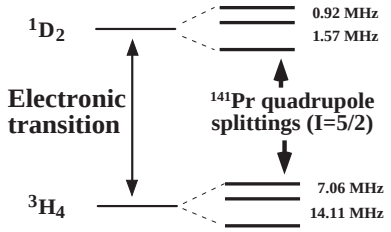

Fig. 8. Relevant level scheme for ^{141}Pr doped into $YAlO_3$.

Figure 8 shows the relevant energy levels for the ^{141}Pr ion doped into the host material $YAlO_3$. The electronic ground state as well as the electronically excited states are split into substates that differ with respect to their nuclear spin coordinates. The separation between these spin states is due to nuclear quadrupole coupling and second order hyperfine coupling, which combine into an effective quadrupole interaction [51, 52].

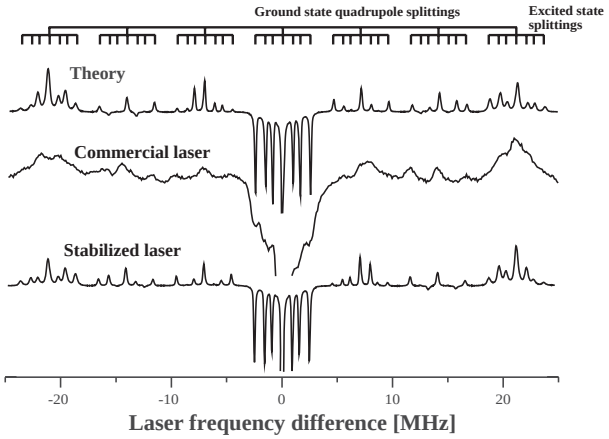

Fig. 9. Holeburning spectrum of Pr:$YAlO_3$.

One approach to measure the NQR transition frequencies is by holeburning spectroscopy, as shown in Figure 9. Since pump and probe laser beam can each

be resonant with nine different transitions (from three ground- to three excited states), the holeburning spectrum, which depends on the difference between the pump and probe laser frequencies, has a total of 81 resonances. A number of these resonances have identical frequencies (e.g. $\nu_P - \nu_T = 0$), resulting in a total of 49 distinguishable frequencies.

The width of each resonance line increases with the laser frequency jitter. As the comparison of the middle and lower traces shows, it is therefore important to use a narrowband laser for measuring these spectra. In this example, the laser linewidth was $\approx 30\,\mathrm{kHz}$; the width of the observed resonance lines was therefore close to the homogeneous width of the optical transition [46].

The amplitudes of the individual resonance lines depend on the optical transition matrix elements and are proportional to the overlap integral $\langle \chi_g | \chi_e \rangle$ of the ground- and excited state nuclear spin states. While the nuclear spin is not involved in the electronic transition, the electronically excited state can have different quantization axes than the ground state if, as in this example, the effective quadrupole interaction changes with the electronic excitation. The precise measurement of the holeburning spectrum allows one then to determine the relative orientation of the principal axis system between the ground- and excited states [46].

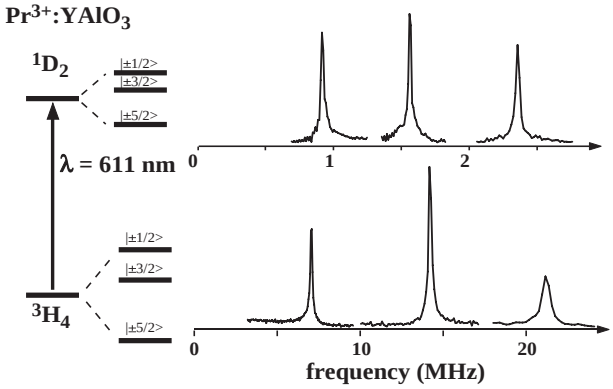

Fig. 10. Raman-heterodyne detected NQR spectra of $Pr:YAlO_3$. All six resonances can be detected in a single wide frequency scan, but the low frequency part, which is associated with the NQR transitions in the electronically excited state has been expanded in the upper part of the figure.

The spectrum can be simplified considerably if the Raman scattering experiment is used instead. In this case, every nuclear spin transition gives rise to a single resonance at the transition frequency. Figure 10 shows an example of a coherent Raman spectrum of $Pr:YAlO_3$ in zero magnetic field, which was recorded by irradiating the optical transition at 611 nm with a laser beam and measuring the Raman-heterodyne signal while sweeping the rf frequency. In

the example shown here, the three NQR transitions at 7, 14, and 21 MHz occur within the electronic ground state, while the three low-frequency transitions (< 3 MHz) belong to the electronically excited state.

4.2 Sign Information

An interesting case of additional information that is unavailable with conventional techniques is the sign of the nuclear quadrupole interaction. As is well known [53], conventional magnetic resonance experiments cannot provide the sign of the quadrupole coupling. In the simplest case of axial symmetry, the Hamiltonian $\mathcal{H}_Q$ of the nuclear quadrupole interaction is given by a coupling constant D times the square of the nuclear spin operator $I_z, \mathcal{H}_Q = DI_z^2$. The coupling constant D is determined by the size of the nuclear quadrupole moment and the electric field gradient. It can be measured either in the absence of a magnetic field, which corresponds to the case of pure quadrupole coupling, or in a high magnetic field, which corresponds to the case of high-field NMR.

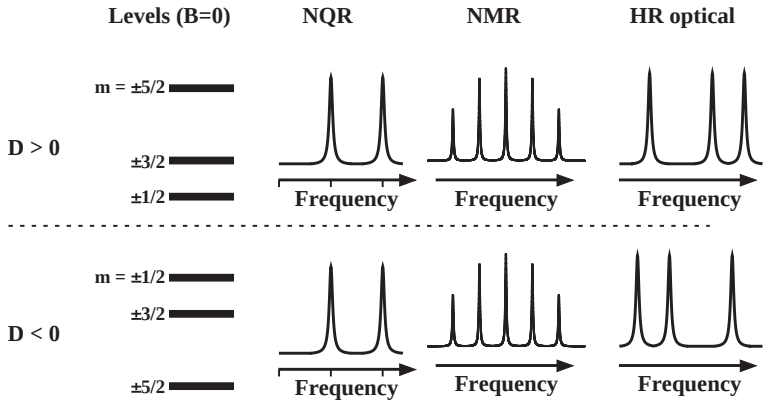

Fig. 11. Measurement of the nuclear quadrupole coupling by NQR, NMR and optical spectroscopy. Only the optical spectra distinguish the sign of the interaction.

Figure 11 shows schematically the NQR (zero magnetic field) and NMR spectra of a spin $I = 5/2$ with axial quadrupole interaction. The spectra for the positive and negative coupling constant D are identical, unless the spin temperature becomes very low or dipolar couplings are resolved. The optical spectrum, however, shown on the right, clearly distinguishes the two cases.

In practice, the inhomogeneous broadening of the optical transitions prevents one from measuring such spectra directly. It is nevertheless possible to use optical and optical-rf double resonance experiments that produce spectra that clearly distinguish the two cases. In the case of Pr^{3+} in the host material $YAlO_3$, the coupling constant turned out to be negative [54].

4.3 Semiconductors

Semiconductors have become a very active area for applications of optically enhanced magnetic resonance. Detection usually relies on changes in the polarization of the photoluminescence. Depending on the sample, the photoluminescence may be dominated by light from trapping sites such as point defects or by recombination of conduction electrons. Point defects usually dominate in indirect semiconductors and amorphous materials [55], while very pure, MBE-grown III/V materials show predominantly interband recombination. Under these conditions, the magnetic resonance signal may originate from the whole sample, while it provides information on localized parts of the material if the recombination is due to defects or heterostructures [56].

Optical pumping occurs by first polarizing the electron spin system [57]. Using a photon energy close to the bandgap, optical excitation creates spin-polarized electron-hole pairs. In bulk materials, this spin polarization is not complete, because optical pumping excites different degenerate transitions that lead to different spin states. In quantum well materials, however, the degeneracy is lifted and electron spin polarization can reach values close to unity [58, 59]. The hyperfine coupling transfers part of this polarization to the nuclear spins [60], which can reach polarizations of more than 50%.

Detection often relies on the Hanle effect: the hyperfine interaction of polarized nuclear spins creates an effective magnetic field, which tends to depolarize the photoluminescence [61, 62]. A number of specific rf excitation schemes have been developed to optimize the optical detection process. The conventional procedure relies on saturation of the nuclear spins, which may lead to power broadening. Other techniques include two-dimensional procedures [63] or beat signals between different isotopes [64]. It is also possible, however, to apply an rf pulse and observe the free induction decay as a modulation of the polarization of the photoluminescence [65].

Materials like GaAs crystallize in a cubic lattice; the symmetry at the site of the nuclei is high enough that the electric field gradient (EFG) tensor vanishes and the three allowed dipole transitions of the I=3/2 nuclei are degenerate in an ideal crystal. Optically detected NMR spectra of quantum wells show quadrupole splittings of several tens of kHz, indicating that the EFG tensor does not vanish in this case. One cause for the nonvanishing quadrupole coupling is a distortion under the influence of mechanical strain [66]. Other possibilities include electrical fields [67]: Since the site symmetry of the nuclei does not include an inversion center, electric fields also can induce a nonvanishing EFG [68, 69].

Figure 12 demonstrates how laser-assisted NMR is capable of measuring small variations of the crystal structure in a multiple quantum well sample with a spatial resolution of some tens of nanometers. The spectra from the individual quantum wells all show distinct quadrupole splittings, which become smaller as the quantum well thickness decreases. At the same time, the

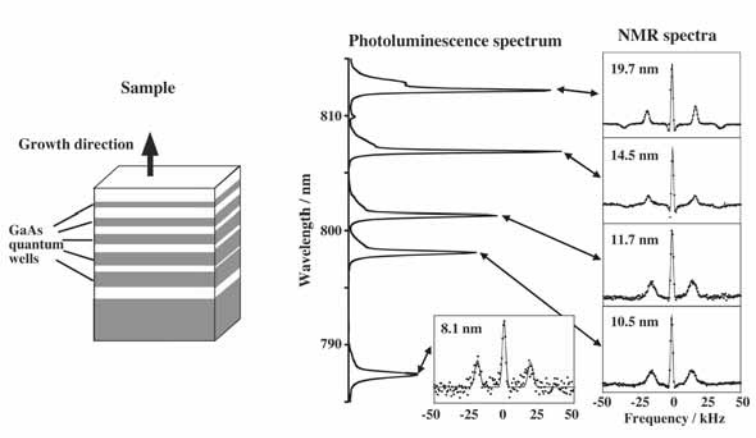

Fig. 12. Variation of quadrupole splittings in a multiple quantum well sample.

width of the satellite lines increases, indicating an increase in the variation of structural distortion and/or electric field distribution.

4.4 Surfaces and Interfaces

Quasi-twodimensional systems have always proved difficult to investigate by conventional NMR, since the number of spins in these systems is quite small [70, 71]. Most of the NMR work on surfaces has therefore concentrated on systems with large surface to volume ratio like Zeolites [72], where most of the atoms are close to the interface. Increasing the spin polarization by optical pumping has significantly improved the sensitivity of this type of experiments. In particular the transfer of spin polarization from optically pumped alkali atoms to Xe nuclear spins [12] has allowed to study the effect of surfaces on the magnetic resonance spectrum [73, 74].

For experiments with oriented surfaces, the use of light for optical pumping as well as for detection brings, apart from the sensitivity advantages, also the possibility to select signal contributions that originate from atoms that are close to the surface. For this purpose, changes in the penetration depth of light with wavelength [75] have been used, but more frequently, the selection is achieved by reflecting a laser beam from the interface being investigated.

The reflection coefficient for the laser beam depends on the refractive indices on both sides of the interface and is therefore affected by atoms close to the interface that are resonant with the laser light. The changes in the reflection coefficient, which can be measured through changes of the amplitude and polarization of the reflected beam contain therefore information on the atoms close to the interface. The combination of optical pumping with this type of optical detection provides sufficient sensitivity, so that it is no longer neces-

sary to use samples with high surface to volume ratios and allows therefore studies on oriented surfaces.

One method that relies on such a technique was used to study nuclear quadrupole resonances of Pr^{3+} in LaF_3 [76]. In this case, the beam was reflected from an optically dense material. The reverse is also possible: if the laser beam undergoes total internal reflection at an interface to an optically less dense medium, an evanescent wave penetrates into the thinner medium by a distance of the order of the optical wavelength. Atoms in this evanescent wave can thus modify the reflected laser beam by absorbing light from it. Similarly, the presence of resonant atoms changes the refractive index of the medium and thereby the reflection coefficient. Both effects can be used for measuring magnetic resonance spectra of atoms that are within an optical wavelength of the reflecting surface [77, 78, 79, 80, 81]

5 EPR

5.1 Experimental Approach

Optically detected magnetic resonance has long been used to study electron spin resonance in various environments. The classical technique measures the photoluminescence while irradiating an EPR transition with a microwave field and sweeping either the frequency or a magnetic field. A number of reviews has appeared that discuss such experiments [82, 28, 83]. We therefore concentrate here on a more recent development, where coherent Raman scattering is used to probe EPR transitions. The examples that we discuss will be mostly metalloproteins, where the information gained with optical-microwave double resonance experiments has proved very useful for identifying the electronic structure of the active centers.

As discussed in section 3.3, coherent Raman scattering is driven by two electromagnetic fields: microwave radiation and laser light, which are tuned to an optical and a magnetic dipole transition in the sample. The sample is placed in a magnetic field to lift the degeneracy of the Zeeman levels. If the laser and microwave fields are both resonant with a transition in the sample, the transmitted laser beam is modulated at the microwave frequency. This modulation is picked up by a fast photodiode The signal can be phase-sensitively down-converted (lock-in detected) with microwaves to yield the optically detected EPR (ODEPR) signal.

While the underlying process can be understood as a coherent Raman process [84], the experiment may also be discussed in terms of modulated circular dichroism [26]. In this model, the resonant microwave irradiation excites transverse magnetisation precessing at the microwave frequency around the static field. As shown in Fig. 13, the precessing magnetisation modulates the circular dichroism and thereby the absorptivity of the sample for circularly

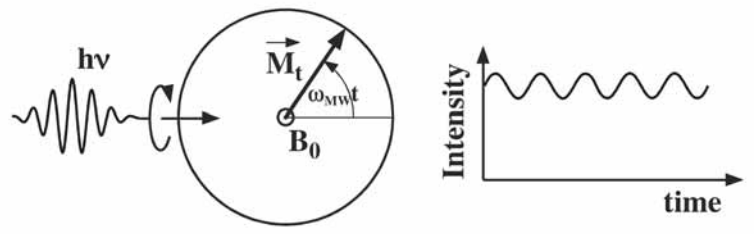

Fig. 13. Continuous wave excitation of EPR creates transverse magnetization M_t that rotates at the angular frequency ω_{MW} around the static magnetic field B_0. The absorption of circularly polarized light is therefore modulated sinusoidally.

polarized light. The modulated signal component is thus proportional to the EPR signal as well as to the magnetic circular dichroism (MCD) of the sample.

From this rotating MCD, we expect a proportionality of the ODEPR signal to the MCD, as well as to the classical EPR signal. The proportionality to MCD was experimentally demonstrated on cytochrome c551 by comparing MCD and ODEPR data of the same sample [26]. The proportionality factor between longitudinal and transverse MCD is determined by the ratio of the transverse vs. longitudinal magnetization components, $\frac{M_{xy}}{M_z} = \omega_{\mathrm{Rabi}} T_2$, where ω_{Rabi} is the Rabi frequency and T_2 is the phase memory time.

5.2 Experimental

The experimental setup required for ODEPR experiments is based on a conventional EPR spectrometer, extended by a laser and some optical components for controlling the laser beam. Detection is based on the modulation signal from a fast photodiode rather than the microwave signal reflected from the resonator [85]. For many samples of interest, the relevant wavelength range cannot be covered by a single laser system. It is then necessary to use different continuous wave lasers including dye, semiconductor, solid state and gas lasers.

While the microwave modulation of the transmitted laser beam can be measured with a single circularly polarized laser beam, it is in practice advantageous to alternate the polarization of the light between left and right circular and use the difference as the actual signal. The modulation can be generated by a photoelastic modulator (PEM) that is placed in the laser beam before it passes through the sample.

The experimental examples that we will discuss are from frozen solutions of metalloproteins. These solutions are placed in a cylindrical cuvette of 0.5 mm inner length and 3 mm inner diameter. The cuvette is mounted inside a rectangular TE_{102} microwave cavity with its microwave magnetic field B_1 parallel to the direction of propagation of the laser beam. The cavity is located inside a helium bath cryostat and has two openings for transmitting the laser beam.

The static magnetic field B_0 of the superconducting split coil magnet is perpendicular to the propagation of the light and thus also to the microwave field B_1. The modulated light (or local oscillator and Raman side-band) is detected with a fast photodiode which is connected to the microwave receiver setup.

ODEPR spectra are measured in field-sweep mode, in close analogy to conventional EPR spectra, except that field modulation is not required. The resulting spectra are therefore directly absorption and dispersion mode, rather than their derivatives. After a proper calibration of the instrument [85], the signal amplitude can be represented as the difference in absorbance ΔA or extinction coefficient $\Delta\epsilon$ between opposite circular polarisations [26].

5.3 Information Content of ODEPR Spectra

The signal generated in this experiment depends on the optical as well as on the magnetic resonance condition. The additional resonance condition, compared to conventional EPR spectroscopy, provides a possible mechanism for distinguishing different paramagnetic centres. This is particularly important when pure samples are difficult or impossible to obtain.

Figure 14 illustrates how the ODEPR spectra provide orientational information. The lineshape of the ODEPR spectrum (Fig. 14 c, d) differs significantly from that of the conventional EPR spectrum (Fig. 14 e). The difference arises from an orientational selectivity: The contribution of every molecule to the total signal is weighted with its MCD sensitivity for the direction of propagation of the laser beam. If a given molecule has the highest MCD sensitivity along the molecular z-axis (Fig. 14 a, b), the main signal contribution (Fig. 14 c) arises from molecules whose z-axis is oriented perpendicular to the static magnetic field. For these molecules, the resonant magnetic field is determined by their g_x and g_y values. The signal is reduced around the g_z position of the spectrum, since molecules with the z-axis along the direction of the magnetic field contribute little to the modulated MCD.

The spectra can be calculated quantitatively by a theory that combines EPR (to calculate spectral positions) and MCD (to calculate the amplitude). We discuss here only the case of an axially symmetric system. We calculate the difference of the extinction coefficients $\Delta\epsilon_x$ (parallel to the laser beam) for circularly polarised light [86, 87, 88] by averaging over the contributions from all possible molecular orientations:

$$\Delta\epsilon_x \propto \int_0^{\pi/2} \sin\theta d\theta \; T(\theta) f(\theta) \left[C_z g_z \frac{g_\perp^2}{g^2} \sin^2\theta + C_\perp g_\perp \left(\frac{g_z^2}{g^2} \cos^2\theta + 1 \right) \right]. \quad (2)$$

Here θ is the angle between the molecular z-axis and the static magnetic field, $T(\theta) = \tanh(g(\theta)\mu_B B_0/2kT)$ is the Boltzmann factor, and $f(\theta)$ describes the transverse magnetization as a function of molecular orientation, amplitude and frequency of the microwave field. $g_\perp$ and g_z are the principal values of the g-matrix perpendicular to and along the molecular z-axis and $g^2 = g_z^2 \cos^2\theta +$

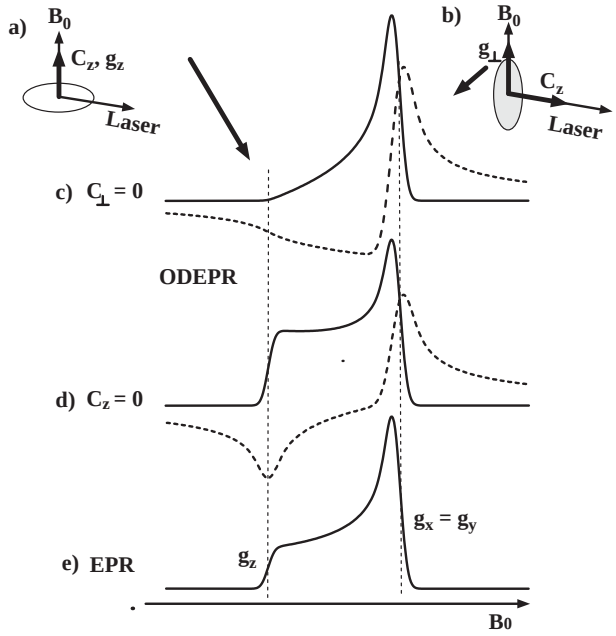

Fig. 14. ODEPR lineshapes contain orientational information. C_z represents the MCD sensitivity in the molecular z-direction and the shaded disk represents the plane of the axially symmetric molecule. a) Molecules with MCD sensitivity only along their z-axis do not contribute when the z-axis is perpendicular to the laser beam. b) They contribute strongly when the z-axis is parallel to the laser beam. c) Calculated ODEPR absorption (solid line) and dispersion (dashed line) of an axially symmetric molecule with MCD sensitivity along its z-axis only. d) Calculated ODEPR when the MCD sensitivity is only perpendicular to the z-axis. e) Calculated conventional EPR absorption.

$g_\perp^2 \sin^2\theta$. $C_\perp$ and C_z are the principal values of the optical anisotropy tensor, which describes the MCD sensitivity.

To obtain the g and C values and the orientation from the experimental spectrum, we fit the conventional as well as the optically detected EPR spectrum with the same parameter set. For the additional analysis, it is convenient to calculate the ratio

$$\frac{C_\perp}{C_z} = \tan\gamma, \tag{3}$$

which parametrises the direction of the optical anisotropy with respect to the g-tensor axis.

A comparison of ODEPR spectra measured at different optical wavelengths shows strong variations of the amplitude and lineshapes of the spectra. This variation arises because the optical anisotropy tensor C is a characteristic property of each optical transition. As the laser interacts with different tran-

sitions, the optical anisotropy changes and, according to (2), also the ODEPR spectrum.

To obtain the anisotropy parameters for each optical transition, we first evaluate the orientation γ as a function of the optical frequency ν. We then fit this angle together with the longitudinal MCD $\Delta\epsilon_z$ (z indicating parallel to B_0) to a sum of contributions i from each optical transition at position p_i with width w_i,

$$\Delta\epsilon_z(\nu) = \sum_i \Delta\epsilon_{zi} \mathrm{e}^{-(\nu-p_i)^2/2w_i^2} \tag{4}$$

and

$$\gamma(\nu) = \arctan\left(\frac{\sum_i C_{\perp i}\ \mathrm{e}^{-(\nu-p_i)^2/2w_i^2}}{\sum_i C_{zi}\ \mathrm{e}^{-(\nu-p_i)^2/2w_i^2}}\right). \tag{5}$$

5.4 Example 1: Azurin

EPR is used extensively to probe the active centres of metalloproteins [89]. Here we use metalloproteins to illustrate the procedure of extracting orientational information from ODEPR spectra of frozen solutions. Our first example is *Pseudomonas aeruginosa* azurin [88]. The conventional EPR spectra of azurin have the typical shape of an axially symmetric system, as shown in Fig. 15 a). The spectrum can be fitted with the following g-values $g_z = 2.26$, $g_\perp = 2.045$, the hyperfine coupling constants $A_z = 172\,\mathrm{MHz}$, $A_\perp = 27\,\mathrm{MHz}$, and the EPR linewidth $\sigma_{\mathrm{EPR}} = 55\,\mathrm{MHz}$.

The corresponding ODEPR spectra (see Fig. 15) are dispersion phase spectra, since the absorption (i.e. in phase) component of the ODEPR signal is strongly saturated under the experimental parameters typically used in these experiments ($T = 1.8\,\mathrm{K}$, microwave power $= 100\,\mathrm{mW}$). This behaviour is exactly analogous to conventional EPR, where the absorption phase of inhomogeneously broadened lines saturates much faster than the dispersion component [90].

A comparison of the ODEPR spectra in Fig. 15 shows that the lineshape varies significantly with the laser wavelength. This variation indicates that different optical transitions are involved, and that the optical anisotropy coefficients are different for these transitions. Fitting the ODEPR spectra with (2), the orientation angle $\gamma = \arctan\frac{C_\perp}{C_z}$ can be determined for each wavelength. Over a large wavelength range, the angle is close to $\gamma = \pi$, indicating that the optical anisotropy reaches a maximum for light propagating parallel to the z-axis of the g-tensor (i.e. molecular symmetry axis) and that the MCD is negative. Close to 800 nm, the MCD becomes positive ($\gamma \approx 2\pi$), and in the region close to 520 nm, the angle reaches $\gamma = \pi/2$.

This variation is a strong indication of an underlying band structure of the optical transitions. To determine this band structure, the theoretical

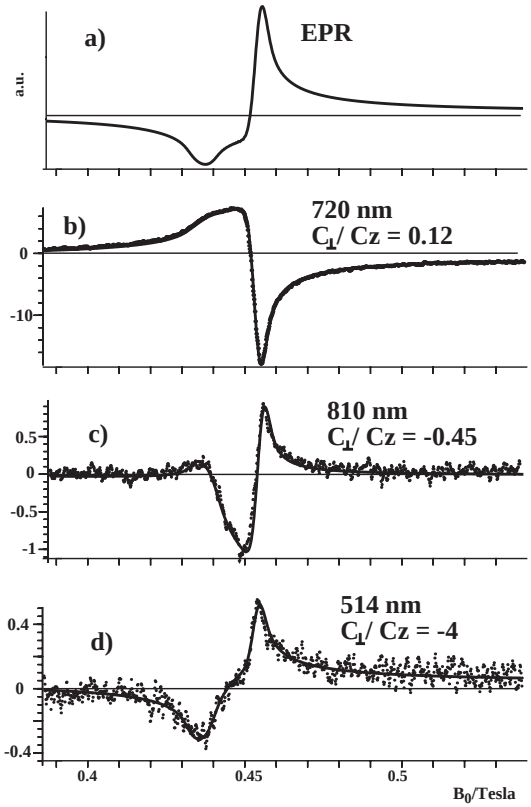

Fig. 15. a) Simulation of conventional EPR absorption (solid line) and dispersion (dashed line). b) to d) Dispersion type ODEPR spectra of azurin at different optical wavelengths in units of $\Delta\epsilon \cdot 10^{-3}\,\mathrm{M}^{-1}\,\mathrm{cm}^{-1}$ (dashed line) and fit curves (solid line) [88].

wavelength-dependence of the orientational angle (5) was fitted to the experimental data simultaneously with a fit of the MCD spectrum. A convincing agreement between the theory and all available experimental data is obtained if six optical transitions are considered (see Fig. 16).

As discussed in detail elsewhere [88]), these optical transitions can be assigned to transitions between electronic states of the metalloprotein. The three higher-energy resonances are charge transfer transitions, the three resonances at lower energy correspond to ligand field transitions. This assignment allows one to calculate the orientation of the optical anisotropy tensor C with respect to the molecular axis system. Since the orientation of the C with respect to the g tensor was determined experimentally, one thereby obtains the orientation of the g-tensor within the molecule. The result obtained for azurin

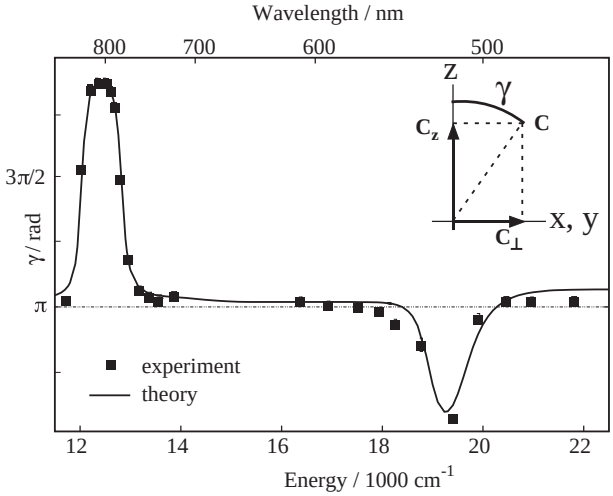

Fig. 16. Variation of the orientational angle γ with the laser wavelength. Filled squares represent experimental data, the solid line the theory. The inset shows the definition of the orientational angle γ in the molecular coordinate system.

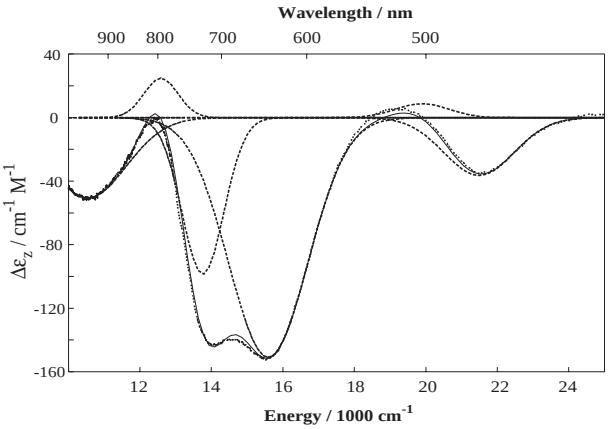

Fig. 17. MCD spectrum of Azurin (solid line) and its decomposition in six Gaussian bands (dotted lines).

agrees well with results from the related compound plastocyanin [91], which had been determined by single crystal EPR.

5.5 Example 2: Rubredoxin

The first high spin system, to which ODEPR was applied, is oxidised rubredoxin from *Clostridium pasteurianum* [92]. This electron transfer protein contains a single high-spin iron sulfur cluster. The optical spectrum has 6 charge

transfer bands in the visible and near UV region. To cover the most interesting part of this spectral range, different lasers with wavelengths between 459 nm and 560 nm were used.

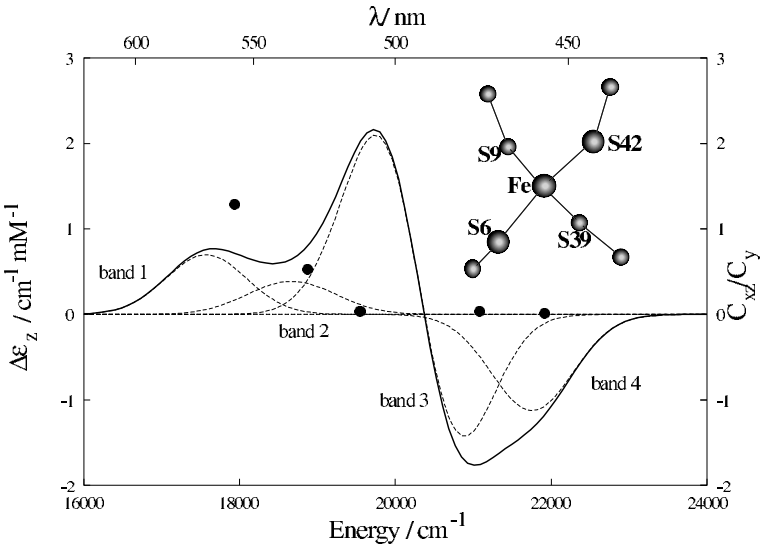

Fig. 18. MCD spectrum (solid line, left hand scale) of Rubredoxin with the four bands (dotted lines). The ratio of C_{xy}/C_y from ODEPR is indicated with dots (right hand scale). The inset shows the active site of rubredoxin, with the iron centre and the four adjacent sulfur atoms. The pseudo-S_4-axis is perpendicular to the plane of drawing.

The EPR spectrum of rubredoxin (conventional and ODEPR) can be explained with a zero field splitting of $D = +46.3\,\mathrm{GHz}$ and a strong rhombic distortion of $E/D = 0.25$, where E is the axial and D the rhombic coefficient. The spectra showed significant deviations from the ideal spectrum expected for these parameters, which can be explained as E/D strain, i.e. a statistical distribution around the mean value of 0.25. This result indicates that the protein conformation is quite variable even in the frozen solution.

The strong variation of the ODEPR lineshape with the optical excitation wavelength allowed us to identify four optical transitions in the wavelength range covered by our measurements. As in the low-spin cases, the ODEPR and MCD spectra were fitted with a single parameter set. Figure 18 shows the MCD of rubredoxin and its decomposition into the four relevant optical transitions.

Even though optical and EPR experiments had already provided most of the relevant parameters in rubredoxin, details like the orientation of the optical and magnetic tensors had remained elusive. With the combination of ODEPR and conventional EPR it was possible to find the positive sign

of the zero field Hamiltonian. Further, the orientation of the g-tensor could be identified and the orientation of the optical symmetry axis was found to be along the direction of largest g-value (perpendicular to the plane of the drawing, inset of Fig. 18).

6 Conclusions

This article summarizes some of the applications of laser radiation to magnetic resonance spectroscopy. The discussion concentrates on applications where the laser light does not modify the sample (apart from the spin system) and therefore excludes, e.g., EPR spectroscopy of photogenerated states. We have distinguished between optical processes that increase the spin polarization and others that are used for the detection. Applications from NMR and EPR were chosen to illustrate the potential of optical techniques. In particular the EPR examples show that the laser is not merely an aid for magnetic resonance, but that the combination of optical and magnetic resonance techniques provides information that is not accessible from separate single resonance optical and magnetic resonance spectra.

7 Acknowledgments

We gratefully acknowledge contributions from many members of the workgroup. Experimental examples were provided by T. Blasberg, B. Enkisch, M. Eickhoff, R. Klieber, and A. Michalowski. Financial support was provided by the *Deutsche Forschungsgemeinschaft*.

References

1. J. Köhler, J. Disselhorst, M. Donckers, E. Groenen, J. Schmidt, W. Moerner: Nature **363**, 242–243 (1993)
2. J. Wrachtrup, C.V. Borczyskowski, J. Bernard, M. Orrit, R. Brown: Nature **363**, 244–245 (1993)
3. J. Wrachtrup, A. Gruber, L. Fleury, C.V. Borczyskowski: Chem. Phys. Lett. **267**, 179–185 (1997)
4. T. Blasberg, D. Suter: Phys. Rev. B **51**, 6309–6318 (1995)
5. A. Kastler: Science **158**, 214–221 (1967)
6. J. Brossel, A. Kastler, J. Winter: J. Phys. Radium **13**, 668–668 (1952)
7. A. Kastler: J. Phys. Rad. **11**, 255–265 (1950)
8. A. Kastler: J. Opt. Soc. Am. B **47**, 460–465 (1957)
9. H. Dehmelt: Phys.Rev. **109**, 381–385 (1958)
10. N. Bigelow, P. Nacher, M. Leduc: J. Phys. II France **2**, 2159–2179 (1992)
11. J. C. Leawoods, D. A. Yablonskiy, B. Saam, D. S. Gierada, M. S. Conradi: Concepts Magn Reson. **13**, 277–293 (2001)

12. W. Happer, E. Miron, S. Schaefer, D. Schreiber, W. v. Wijngaarden, X. Zeng: Phys. Rev. A **29**, 3092–3110 (1984)
13. D. Raftery, H. Long, T. Meersmann, P. Grandinetti, L. Reven, A. Pines: Phys. Rev. Lett. **66**, 584–587 (1991)
14. H. Jänsch, T. Hof, U. Ruth, J. Schmidt, D. Stahl, D. Fick: Chem. Phys. Lett. **296**, 146–150 (1998)
15. H.-U. Kauczor, M. Ebert, K.-F. Kreitner, H. Nilgens, R. Surkau, W. Heil, D. Hofmann, E. W. Otten, M. Thelen: JMRI **7**, 538–543 (1997)
16. D. Levron, D.K. Walter, S. Appelt, R.J. Fitzgerald, D.Kahn, S.E. Korbly, K.L. Sauer, W. Happer, T.L. Earles, L.J. Mawst, D. Botez, M. Harvey, L. DiMarco, J.C. Connolly, H.E. Möller, X.J. Chen, G.P. Cofer, G.A. Johnson: Magnetic resonance imaging of hyperpolarized 129Xe produced by spin exchange with diode-laser pumped cs. apl **73**, 2666–2668 (1998)
17. G. Cates, D. Benton, M. Gatzke, W. Happer, K. Hasson, N. Newbury: Phys. Rev. Lett. **65**, 2591–2594 (1990)
18. C. Bowers, H. Long, T. Pietrass, H. Gaede, A. Pines: Chem. Phys. Lett. **205**, 168–170 (1993)
19. F. Bitter: Phys. Rev. **76**, 833–835 (1949)
20. H.G. Dehmelt: Phys. Rev. **105**, 1924–1925 (1957)
21. E.W. Bell, A.L. Bloom: Phys. Rev. **107**, 1559–1565 (1957)
22. N. Bloembergen, P.S. Pershan, L.R. Wilcox: Phys. Rev. **120**, 2014–2023 (1960)
23. I. Wieder: Phys. Rev. Lett. **3**, 468–470 (1959)
24. C.P. Barrett, J. Peterson, C. Greenwood, A.J. Thomson: J. Am. Chem. Soc. **108**, 3170–3177 (1986)
25. S.J. Bingham, D. Suter, A. Schweiger, A.J. Thomson: Chem. Phys. Letters **266**, 543–547 (1997)
26. B. Börger, S.J. Bingham, J. Gutschank, M.O. Schweika, D. Suter: J. Chem. Phys. **111**, (18), 8565–8568 (1999)
27. A.B. Dennison: Magnet. Resonance Rev. **2**, (1), 1–33 (1973)
28. R.H. Clarke, editor: *Triplet State ODMR Spectroscopy* (John Wiley, New York 1982)
29. J. Brossel, F. Bitter: Phys. Rev. **86**, 308–316 (1952)
30. F. Jelezko, I. Popa, A. Gruber, C. Tietz, J. Wrachtrup, A. Nizovtsev, S. Kilin: Appl. Phys. Lett. **81**, 2160–2162 (2002)
31. W. Hanle: Z. Physik **30**, 93–105 (1924)
32. N. Bloembergen, Y. Zou, L. Rothberg: Phys. Rev. Lett. **54**, 186–188 (1985)
33. J. Brossel, S. Geschwind, A. Schawlow: Phys. Rev. Lett. **3**, 548 (1959)
34. D. Paget, G. Lampel, B. Sapoval, V. Safarov: Phys. Rev. B **15**, 5780–5796 (1977)
35. C. Raman, K. Krishnan: Nature **121**, 501–502 (1928)
36. J.A. Giordmaine, W. Kaiser: Phys. Rev. **144**, (2) (1966)
37. Y. Bai, R. Kachru: Phys. Rev. Lett. **67**, 1859–1862 (1991)
38. N. Wong, E. Kintzer, J. Mlynek, R. DeVoe, R. Brewer: Phys. Rev. B **28**, 4993–5010 (1983)
39. R. Shelby, C. Yannoni, R. Macfarlane: Phys. Rev. Lett. **41**, 1739–1742 (1978)
40. L. Erickson: Phys. Rev. B **43**, 12723–12728 (1991)
41. R. Shelby, A. Tropper, R. Harley, R. Macfarlane: Opt. Lett. **8**, 304–306 (1983)
42. R. Shelby, R. Macfarlane: J. Luminesc. **31**, 839–844 (1984)
43. T. Blasberg, D. Suter: Optics Commun. **109**, 133–138 (1994)

44. S. Völker: Ann. Rev. Phys. Chem. **40**, 499–530 (1989)
45. N.B. Manson, N. Rigby, B. Lou, J.P. Martin: J. Luminesc. **53**, 251–254 (1992)
46. R. Klieber, A. Michalowski, R. Neuhaus, D. Suter: Phys. Rev. B **67**, 184103 (2003)
47. Y. Chen, K. Chiang, S. Hartmann: Phys. Rev. B **21**, 40–47 (1980)
48. A. Szabo: J. Opt. Soc. Am. B **3**, 514–522 (1986)
49. R.M. Macfarlane: Journal of Luminescence **100**, 1–20 (2002)
50. A. Kaplyanskii, R. Macfarlane: *Spectroscopy of solids containing rare earth ions* (Elsevier 1987)
51. B. Bleaney: Physica **69**, 317–329 (1973)
52. M. Teplov: Sov. Phys. JETP **26**, 872 (1968)
53. A. Abragam: *The Principles of Nuclear Magnetism* (Oxford University Press, Oxford 1961)
54. T. Blasberg, D. Suter: Phys. Rev. B **48**, 9524–9527 (1993)
55. K. Morigaki: Jap. Journal of Applied Physics **22**, 375–388 (1983)
56. E. Glaser, J. Trombetta, T. Kennedy, S. Prokes, O. Glembocki, K. Wang, C. Chern: Phys. Rev. Lett. **65**, 1247–1250 (1990)
57. M. D'Yakonov, V. Perel: Sov. Phys. JETP **33**, 1053–1059 (1971)
58. G. Flinn, R. Harley, M. Snelling, A. Tropper, T. Kerr: J. Luminesc. **45**, 218–220 (1990)
59. T. Uenoyama, L. Sham: Phys. Rev. Lett. **64**, 3070–3073 (1990)
60. M. D'Yakonov, V. Perel: Sov. Phys. JETP **36**, 995–1000 (1973)
61. D. Paget: Phys. Rev. B **24**, 3776–3793 (1981)
62. M. Krapf, G. Denninger, H. Pascher, G. Weimann, W. Schlapp: Solid State Comm. **78**, 459–464 (1991)
63. S.K. Buratto, D.N. Shykind, D.P. Weitekamp: Phys. Rev. B **44**, 9035–9038 (1991)
64. J. Marohn, P. Carson, J. Hwang, M. Miller, D. Shykind, D. Weitekamp: Phys. Rev. Lett. **75**, 1364–1367 (1995)
65. M. Eickhoff, D. Suter: J. Mag. Res. **166**, 69–75 (2004)
66. D. Guerrier, R.T. Harley: Appl. Phys. Lett. **70**, 1739–1741 (1997)
67. M. Eickhoff, B. Lenzmann, D. Suter, S.E. Hayes, A.D. Wieck: Phys. Rev. B **67**, 085308 (2003)
68. D. Gill. N. Bloembergen: Phys. Rev. **129**, 2398–2403 (1963)
69. K. Dumas, F. Soest, A. Sher, E. Swiggard: Phys. Rev. B **20**, 4406–4415 (1979)
70. C. Slichter: Ann. Rev. Phys. Chem. **37**, 25 (1986)
71. T. Duncan, C. Dybowski: Surf. Science Reports **1**, 157 (1981)
72. B. Chmelka, D. Raftery, A. McCormick, L. DeMenorval, R. Levine, A. Pines: Phys. Rev. Lett. **66**, 580 (1991)
73. Z. Wu, W. Happer, M. Kitano, J. Daniels: Phys. Rev. A **42**, 2774 (1990)
74. R. Butscher, G. Wäckerle, M. Mehring: J. Chem. Phys. **100**, 6923–6933 (1994)
75. D.J. Lepine: Phys. Rev. B **6**, 436–441 (1972)
76. M. Lukac, E. Hahn: J. Luminesc. **42**, 257–265 (1988)
77. D. Suter, J. Aebersold, J. Mlynek: Opt. Commun. **84**, 269–274 (1991)
78. S. Grafström, T. Blasberg, D. Suter: J. Opt. Soc. Am. B **13**, 3–10 (1994)
79. S. Grafström, D. Suter: Optics Letters **20**, 2134–2136 (1995)
80. S. Grafström, D. Suter: Phys. Rev. A **54**, 2169–2179 (1996)
81. S. Grafström, D. Suter: Zeitschrift für Physik D **38**, 119–132 (1996)
82. B. Cavenett: Adv.Phys. **30**, 475–538 (1981)

83. J. Köhler: Physics Reports **310**, 261–339 (1999)
84. M.O. Schweika-Kresimon, J.Gutschank, D. Suter: Phys. Rev. A **66**, (4), 043816 (2002)
85. S.J. Bingham, B. Börger, D. Suter, A.J. Thomson: Rev. Sci. Instrum. **69**, (9), 3403–3409 (1998)
86. S.J. Bingham, B. Börger, J. Gutschank, D. Suter, A.J. Thomson: JBIC **5**, 30–35 (2000)
87. S.J. Bingham, J. Gutschank, B. Börger, D. Suter, A.J. Thomson: J. Chem. Phys. **113**, 4331–4339 (2000)
88. B. Börger, J. Gutschank, D. Suter, A.J. Thomson, S.J. Bingham: J. Am. Chem. Soc. **123**, 2334–2339 (2001)
89. G. Palmer: *Methods for Determining Metal Ion Environments in Proteins* In Vol. 2 of *Advances in Inorganic Biochemistry*, Chapter in 6 *Electron Paramagnetic Resonance* (Elsevier, Amsterdam 1980)
90. A.M. Portis: Phys. Rev. **91**, (5), 1071–1078 (1953)
91. K.W. Penfield, R.R. Gay, R.S. Himmelwright, N.C. Eickman, V.A. Norris, H.C. Freeman, E.I. Solomon: J. Am. Chem. Soc. **103**, 4382–4388 (1981)
92. B. Börger, D. Suter: J. Chem. Phys. **115**, (21), 9821–9826 (2001)